TITLE
Multi-scale modelling of the feto-placental vasculature

Authors: AR Clark[1], M Lin[1], M Tawhai[1], R Saghian[1], JL James[2]

Address:

[1]Auckland Bioengineering Institute, University of Auckland, Auckland, New Zealand.

[2]Department of Obstetrics & Gynaecology, University of Auckland, Auckland, New Zealand

Corresponding Author:

A. R. Clark

Auckland Bioengineering Institute

The University of Auckland

Auckland

New Zealand

Email alys.clark@auckland.ac.nz

Abstract

The placenta provides all the nutrients required for the fetus through pregnancy. It develops dynamically and to avoid rejection of the fetus there is no mixing of fetal and maternal blood, rather the branched placental villi 'bathe' in blood supplied from the uterine arteries. Within the villi, the feto-placental vasculature also develops a complex branching structure in order to maximise exchange between the placental and maternal circulations. To understand the development of the placenta we must translate functional information across spatial scales including the interaction between macro- and micro-scale haemodynamics and account for the effects of a dynamically and rapidly changing structure through the time-course of pregnancy. Here we present steps toward an anatomically based and multi-scale approach to modelling the feto-placental circulation. We assess the effect of the location of cord insertion on feto-placental blood flow resistance and flow heterogeneity and show that although cord insertion does not appear to directly influence feto-placental resistance, the heterogeneity of flow in the placenta is predicted to increase from a 19.4% coefficient of variation with central cord insertion to 23.3% when the cord is inserted 2cm from the edge of the placenta. Model geometries with spheroidal and ellipsoidal shapes, but the same volume showed no significant differences in flow resistance or heterogeneity implying that normal asymmetry in shape does not affect placental efficiency. However, the size and number of small capillary vessels is predicted to have a large effect on feto-placental resistance and flow heterogeneity. Using this new model as an example, we highlight the importance of taking an integrated multi-disciplinary and multi-scale approach to understand development of the placenta.

Key index words or phrases (3-6 choices)

Placenta, pregnancy, feto-placental circulation, computational model, vascular structure, multi-scale

Summary

The placenta is a dynamically developing organ, which provides all the nutrients that the fetus needs through pregnancy. To efficient exchange nutrients and waste it develops a complex branching structure to maximise exchange between the placental and maternal circulations. Here we present steps toward an anatomically based and multi-scale approach to modelling the placental circulation, which translates structural data to functional information across spatial scales including the interaction between macro- and micro-scale haemodynamics. We show the importance of micro-scale structure to whole placental resistance, highlighting the importance of taking an integrated multi-scale approach to understand development of the placenta.

1. Introduction

Successful placental development is critical for fetal development. The placenta is a fetal exchange organ that provides essential nutrients and gases to the fetus and removes fetal waste. It achieves this by having an extensively branched tree-like structure known as the villous tree, within which resides a further branched network of fetal blood vessels. The placental villi bathe in maternal blood, and thus the fetal and maternal circulations are never in direct contact, but rather exchange occurs across a thin layer of placental specific epithelial cells called trophoblast that form the outer surface of the placenta. Thus, nutrient exchange between the maternal and fetal circulations across this barrier may be affected by the dynamics of maternal and fetal blood flow, as well as mixing of maternal blood in the space between the villous tissue. In severely pathological pregnancies abnormalities have been found in the structure and function of this gas exchange tissue, including sparser capillary networks (1, 2) and increased numbers of 'redundant' capillary connections (2, 3) leading to impaired fetal growth. However, the mechanisms that contribute to these abnormalities, and the influence of more subtle structural variations on the efficiency of the placenta are largely unknown.

The structure and function of the feto-placental vasculature throughout gestation is defined by behaviours at multiple spatial and temporal scales. A schematic of the structure of the placental vasculature is given in Figure 1. The largest placental blood vessels (termed the chorionic vessels) are macroscopic. The arteries at the umbilical cord insertion point measure up to 5 mm in diameter (4), in normal placentas they branch in a mostly dichotomous manner to ultimately form approximately 60-100 chorionic arteries as small as 0.8mm in diameter that branch into the villous tissue (4-6). As these vessels extend into the underlying villus tree, they branch further into multiple arterioles and venules that terminate in a dense network of capillary 'convolutes' (7-9). In terms of temporal scale, the placenta is constantly developing throughout gestation, with significant blood flow in the feto-placental circulation at approximately 8 weeks of gestation, and flow increasing through to term (10, 11). This increase in blood flow happens over a relatively long time scale compared with nutrient transport kinetics so appropriate timeframes must be considered in modelling developmental processes. In vivo assessment of pathology in the placental vasculature relies on Doppler ultrasonography at the level of the umbilical artery, where flow velocity waveforms and measured pulsatility indicate both fetal cardiac function and the resistance of the placental vasculature (12).

<INSERT FIGURE 1>

As well as the structure of the feto-placental vasculature itself, the size and shape of the whole placenta has been associated with pregnancy complications such as fetal growth restriction, which itself has long-term cardiovascular consequences for the affected babies (13). The gross morphology of the placenta is believed to be established by the end of the first trimester (14). Although the human placenta is classified as discoidal organ (15) placental shape varies between individuals. The shape of an average 'normal' placenta at term has been described as close to a circular in cross section, or having an ellipsoidal shape (12, 16) and placental volumes estimated *in vivo* at term are approximately 428 cm^3 (17). Deviations from normal placental size and shape have received particular interest in recent years as potential markers of placental health or efficiency (16, 18-21). Most studies have suggested that deviations in shape (other than extreme) are not significantly correlated with pathologies (such as pregnancy induced hypertension, gestational diabetes, small for gestational age fetuses) (16, 18), but one study has suggested that an ellipsoidal placental shape in female offspring could be linked to high blood pressure in later life (21). On the other hand placental size appears to be a key factor in outcome, with placentas from pregnancies affected by fetal growth restriction typically being small in size (16, 18-20). In addition, the point of umbilical

cord insertion appears to affect placental function, with cord insertion near the outer boundary of the placenta (marginal insertion) resulting in a more asymmetric chorionic vessel structure (4, 6), which has been linked to fetal growth restriction, still birth and neonatal death (22).

It is clear from clinical and anatomic studies of the placenta and its vasculature that its efficiency is determined by several interacting factors. These include the structure of the vasculature from the large vessels of the chorionic plate, through to the small capillary vessels that contribute to gas exchange, and the size and shape of the placenta itself. As the placenta is an organ that is inaccessible to high resolution *in vivo* measurements of structure and function, we rely on indirect measurements of the function of its vasculature (such as Doppler ultrasound of the umbilical artery), or post-partum studies to find correlations between structure and function. Translating animal models of the placenta to human function is problematic as the anatomical structure of the exchange surface and vascular network in humans differs significantly from many common animal models (23, 24). Computational models provide a means to relate structure to function in the placental vasculature and ultimately to better understand human pregnancy. However, to date models have focused on a single level of the placental vasculature such as the structure of the chorionic vessels, or have studied the whole fetal vasculature by simplifying the placental vasculature into a single component (or resistance). Here we review existing computational models of the feto-placental vasculature at each spatial scale of interest and propose a framework for modelling the feto-placental vasculature that includes anatomical detail from the point of cord insertion through the villous capillaries.

2. Existing models of the feto-placental vasculature

2.1. Chorionic vessels

Many computational models of the feto-placental vasculature focus on the structure and function of the chorionic vessels. The size and structure of these vessels makes them easy to assess and detailed morphometric studies have been conducted to describe the branching structure of the chorionic vasculature (4-6). The flow of blood in this branching structure has been investigated using 3D computational fluid dynamics (CFD) to examine small subsets of vessels, consisting of approximately 5 vessels, in order to assess the importance of chorionic vessel branching asymmetry with representative pressure and flow boundary conditions assumed at the inlets and outlets (25). To solve for blood flow in the entire chorionic tree Franke et al. (26) used a simplified 1D representation of flow by neglecting arterial curvature and assuming axi-symmetry in flow. As the villous trees were not explicitly represented in this model boundary conditions were assumed at the inlet of each villous tree, thus the villus structure was not described.

2.2. Villous vessels

The vessels within the villous tree are less accessible to measurement than the larger chorionic vessels. However, their branching structure has been studied in some detail (7, 8). No existing model explicitly incorporates this structure. However, Yang et al. (27) incorporate multiple generations of the villous vasculature in an anatomically based model of the mouse placental arteries constructed from micro computed tomography (micro-CT) imaging. To incorporate a large number of arteries into this model, the fluid dynamics of blood flow within the vasculature was simplified to a steady-state Poiseuille flow. A constant blood pressure of 0 mmHg was assumed at each terminal vessel, which represents the limit of micro-CT resolution. This means that each terminal vessel could lie in different anatomical levels, and the smallest high resistance vessels are neglected.

2.3. System models

A major drawback of considering the largest feto-placental vessels in isolation in a computational model is that each 'terminal' branch of the vasculature must be assigned an assumed boundary condition. These conditions cannot be measured, as the size of blood vessels at which boundary conditions must be applied is too small to visualise in functional imaging during pregnancy. To understand the implications of each contributor to feto-placental vascular resistance, we must consider the whole system. Simple models of the placental vasculature have been developed that include representations of the entire feto-placental vasculature from the umbilical arteries to the umbilical vein (28, 29). These models have the advantage over models that represent an isolated sub-region of the placenta, in that flow velocity waveforms can be measured in the umbilical, and so boundary conditions defining pressure and flow in the umbilical vessels can be readily defined. However, since the placenta contains many thousands of blood vessels (7), the fluid dynamics of blood flow in the system, the geometry, or both, must be simplified to attain a computationally tractable model of the function of the system. In existing studies the asymmetric structure of the placental vasculature is simplified to a symmetrically branching tree with 14-15 generations at term (28), or a single unit (29), and by solving for wave propagation through the system. With these models, gestational age can be accounted for by simply changing the number of branching generations and the calibre of vessels, but key structure-function relationships are lost in geometric simplification.

By simplifying model geometries, powerful predictions can be made regarding placental function using simple, easy to solve, models. By modelling a subunit of the placenta as a homogenous mix of blood vessels and intra-villous space in a hemisphere Chernyavsky et al. (30) predicted blood flow and oxygen uptake in placental tissue analytically. The study used this simple model to hypothesise how changes in spiral artery blood flow and calibre could influence the shear stress felt by placental tissue, which could result in adaptive remodelling on the placental tissue and a change in placental efficiency. By considering the placenta as four compartments (with no explicit geometrical representation), Hill et al. (31) were able to implement a detailed model of carbon dioxide and oxygen transport in the placenta. Including this functional, rather than geometric, detail allowed assessment of the effect of haemoglobin levels and the balance of maternal to fetal blood flow on exchange. Also using a compartment model Sengers et al. (32) produced a detailed model of amino acid transport between maternal and fetal blood. These geometrically simple models allow great insight into the function of an organ system but do not allow for the significant heterogeneity in function that can occur within that organ.

An alternative approach is to include structural heterogeneity in a model, which increases computational complexity but allows comprehensive assessments of structure-function relationships in an organ. By taking a multi-scale approach to modelling the relationship between structure and function in large vascular networks, recent studies have been able to accurately predict the effects of small-scale perturbations to flow on vascular resistance and distribution of blood flow in other organs such as the lung (33). Here we take a similar approach to build a multi-scale picture of function in the feto-placental vasculature that can allow us to assess function in an anatomically realistic model of the placenta, whilst retaining computational tractability.

3. Methods

Here we describe a multi-scale computational model of the feto-placental vasculature of an 'average' placenta, based on structural descriptions across spatial scales given in the literature. Several aspects of the model can be 'individualised' based on measurements that can be made *in vivo* or post-partum. However, describing an average placenta computationally provides the opportunity to assess several important questions such as: What are the implications of marginal cord insertion on the resistance of the feto-placental

vasculature and the distribution of flow within the placenta? How much disruption to capillary structure is necessary before a change in haemodynamics at the level of the umbilical cord can be detected?

3.1. Placental shape

Quantitative assessments of placental shape in normal uncomplicated pregnancies have cumulated in a description of the placenta as a spheroidal or ellipsoidal organ (12, 16, 18). Salafia et al. (18) described the median post-partum placenta as round with radius 9.07 cm. *In vivo* measurements of placental volume (17), and post-partum estimates (34) are consistent with one another at 400-500 cm^3. Using the median placental radius of Salafia et al., the median volume of de Paula et al. (17) (428 cm^3), and assuming that the placenta is a uniform oblate spheroid we can write the volume of the placenta (V) as

$$V = \frac{4}{3}\pi r^2 t, \quad (1)$$

where r is the radius of the placenta and τ is half of the placental thickness. We can then estimate the thickness of the placenta to be 2.48 cm, which compares well to *ex vivo* estimates of placental thickness (5). There is some evidence that placental thickness *in vivo* is larger than *ex vivo* (5), this would reduce the diameter of the placenta *in vivo* if the volume of the placenta remains consistent as suggested by *in vivo* and *ex vivo* studies. Similarly, there is evidence that the average placenta is ellipsoidal rather than spheroidal (16). This is imposed on the placental geometry, while retaining volume by introducing a major (r_{maj}) and minor (r_{min}) radius on the description of the geometry.

To allow in the future for definition of non-uniform placental shapes or individualised placental shapes from 3D ultrasound (17, 20) a geometrical shape model (called a finite element mesh) was constructed to represent the placental volume. The shape model represents an oblate spheroid or ellipsoid, and was obtained by fitting a template shape to data clouds representing the placental surface. Details of shape fitting follow Fernandez et al. (35) and are outlined in Appendix A.1.

Three cases were considered:

1. A spheroidal placenta (a flattened 3D shape with spherical cross-section) with cord insertion at the centre representing the 'average' placenta described by Salafia et al. (18)
2. A placenta with the same spheroidal shape but with cord insertion close to the placental margin (2cm from the edge of the placenta). This represents the more asymmetric placentas associated with non-central cord insertion (4-6, 36).
3. An ellipsoidal (a flattened 3D shape with elliptical cross section) placenta with r_{maj}/r_{min} =1.68, which reflects typical eccentricities of placentas assessed by Salafia et al. (18).

By using computational tools to simulate perfusion within generated vasculatures in each of these geometries we aim to assess the influence of gross placental structure on the efficiency of the placenta to transport fetal blood to the peripheral gas exchange tissue.

3.2. Chorionic vessels

The chorionic arteries begin at the point of umbilical cord insertion and branch through 6-8 generations to feed approximately 60-100 villous trees (4, 36). The branching of the chorionic

arteries are described as a combination of dichotomous, where branching is largely symmetric, and monopodial, where branches form large major pathways with small minor branches (termed the intraplacental vessels (37)) arising at close to right angles from the major branches to supply the placental tissue (4-6, 36). Parameterisation of the algorithm employed to generate chorionic vessels as described below and in Appendix A.2 results in 92 villous trees, consistent with the number identified and used in models from previous studies (4, 36)

The two arteries at umbilical cord insertion point are modelled as lines representing the vessel centreline over a small portion of their length (two linear elements, equidistant from the point of cord insertion). These inlet arteries, representing the distal ends of the umbilical arteries are defined to be 20 mm long and 4 mm in diameter (based on estimates from 1-5.6mm in diameter (4, 8)), thus they add a constant known resistance to that of the placental villus arteries to be generated. The umbilical arteries terminate at the surface of the placental shape, which acts as the 'chorionic surface' over which chorionic arteries are generated. Seed points were defined on the chorionic surface, towards which an asymmetric tree was grown. Thirty-two seed points, equally spaced over the chorionic surface, were defined And a Monte Carlo method described by Wang et al. (38) was implemented in CMISS (www.cmiss.org) to generate an 'area filling' bifurcating system of chorionic vessels. Details of seed point generation and the growing algorithm are given in Appendix A.2 and the algorithm is schematically illustrated in Figure 2. The asymmetry in the chorionic vessels is then dependent on the shape of the chorionic surface and the location of the umbilical cord insertion. Each chorionic vessel is then represented by a single finite element defined by two nodes (its start and end point) with vessel radii as defined in Table 1.

<INSERT FIGURE 2 HERE>

<INSERT TABLE 1 HERE>

Intraplacental vessels were generated to branch from the main chorionic arteries at the midpoint of each artery by refining each chorionic element once at its midpoint and generating an additional element orientated at 90^{o} to its parent branch (4-6, 36), extending 2 mm into the placenta (7). A bifurcation between a chorionic vessel and intraplacental vessel is shown in Figure 3a.

<INSERT FIGURE 3 HERE>

3.3 Villous vessels

Beyond the chorionic vessels the placenta consists of several independent units, known as fetal cotyledons containing a villous tree (37). The villous trees in turn contain the placental villous blood vessels, which follow the branching structure of the villous trees for several generations before approaching the capillary structures which fill the distal ends of the villous trees (7, 8).

Branching component: The branching component of the placental villous vasculature is described in some detail in the literature (7-9). However, no single study gives a comprehensive description of its branching structure. From the intraplacental vessels (or the stem of the villous tree) there are up to 15 generations of branching villi and vessels (7, 8), and the structure of these vessels is asymmetric (terminal capillary conduits branch from vessels throughout the tree from near its stem to the periphery) (8, 9). To simulate this branching structure a volume filling branching algorithm based on the area-filling algorithm used to generate the chorionic vessels is implemented. The generalisation of the area filling algorithm to volumes is described by Tawhai et al. (39) who used the algorithm to generate

morphometrically realistic pulmonary airway trees and is detailed in Appendix A.2. The input parameters to this algorithm control the number of branching generations and asymmetry of the tree and are: the number of seed points, the minimum length of an individual branch, the maximum branch angle of a child branch from its parent's axis, and the fractional distance to the centre of mass that each vessel grows (Figure 2). There is no consensus on the number of blood vessels in a villous tree, but several studies agree that the villous structure branches up to 15 times in a single pathway (7, 8). The Strahler branching ratio provides a measure of asymmetry and is defined by assigning each branch in a tree structure a Strahler order (7), counting the number of branches in each order (b_N), and obtaining the gradient of the straight line fitted to $\log(b_N)$ plotted against order. A symmetric tree has a Strahler branching ratio of 2.0. The Strahler branching ratios at different stages of gestation were estimated from trees reconstructed by Kosanke et al. (9) and range from 2.19 to 2.83 suggesting significant asymmetry[1]. Indeed calculating the resistance of the arterial vasculature as defined in an idealised symmetric model with 15 branching generations (7), and assuming Poiseulle resistance in each vessel results in an estimate of villous vascular resistance that is 3-fold higher than estimates of the whole placental resistance calculated from measurements of umbilical blood pressures and placental blood flow. Therefore, to construct a model of the branching component of the villous vasculature, the parameters of the volume filling branching algorithm were successively altered to obtain approximately 15 post-chorionic branching generations and to match as closely as possible the branching ratio range obtained from the data of Kosanke et al. (9). This results in a range of possible seed point densities and thus an additional fitting step was implemented to match data regarding placental vascular resistance in the normal case. Diameters of vessels are reduced at each order to achieve a vessel diameter for arteries feeding terminal convolutes of 0.030 mm (7). Examples of generated branching structures including chorionic vessels are shown in Figure 3 (b-c).

Capillary pathways: Beyond the branching component of the villous trees lies a tortuous network of capillary pathways. Confocal laser scanning microscopy of the capillary convolutes indicate several parallel pathways between arteries and veins with variation in the number and connectivity of pathways in pathology (3, 40). In a model that comprises the whole placental vasculature it is not feasible computationally to incorporate each capillary pathway individually. Therefore, the vasculature of the intermediate villi and their associated terminal convolutes is represented in the model as a single resistance estimated from the known morphology of the parallel capillary pathways. This grouping of many pathways into a single model is termed a lumped-parameter model. The, most distal vessel of each generated stem villous tree (that feeds intermediate villi and capillary convolutes) branches to 8-10 mature intermediate villous vessels (7). Assuming a symmetric branching structure to intermediate villi results in, on average, 3 generations of intermediate villous arteries. Each intermediate villous vessel arises convoluted capillary branches which have a cumulative length of 3 mm (7). By making the simplifying assumption that each intermediate villous artery is associated with *n* parallel capillary pathways that contribute to gas exchange we can formulate a simple model of the terminal component of the villous tree (Figure 4). Each intermediate villous artery is described as a cylindrical vessel of diameter 0.030 mm, and length 1.5 mm and there assumed to be 3 symmetric generations of intermediate villous arteries, each giving rise to *n* capillary conduits of length 3 mm and which arise at equal distances along its length (Figure 4). The data of Leiser et al. (7) suggest that in a normal placenta n=6. Resistances are calculated, assuming Poiseuille flow, in the same manner as described by Clark et al. (41) for a similar vessel structure with a single capillary connection at each generation, by summing component resistance of each symmetric generation in parallel and then summing all resistances in series (more details are given in Appendix A.3). This provides an effective resistance for each terminal unit without explicit generation of a finite element to represent each capillary unit.

[1] Note that the 'branching ratios' calculated by Kosanke et al. are not Strahler branching ratios as defined here and these values are calculated by reconstructing the trees measured in that study.

<INSERT FIGURE 4 HERE>

Placental venous system: To complete the circuit we include a representation of the placental venous system. For simplicity, we assume that the placental veins follow the arteries, but are larger than the arteries with each placental vein assumed to be two times the calibre of its associated artery (literature descriptions estimate veins are 1-2.5 times larger than arteries (18).

3.4. Perfusion simulation

As the nature of the placental vasculature is multi-scale spatially and temporally, the type of model required to describe perfusion in the system depends on the application of the model. Steady state models may be sufficient to represent 'efficiency' in terms of placental resistance to blood flow and the distribution of blood available to gas exchange. However, pulsatile models of blood flow will be required to simulate Doppler indices of blood flow. Here we have simulated steady-state blood flow to demonstrate the geometric model's capability of predicting resistance and heterogeneity in flow, as measures of efficiency. Pressure boundary conditions are defined at the umbilical vein (20 mmHg or 2660 Pa (42)) and blood flow into the placenta is fixed at approximately 21% of the fetal cardiac output (250 ml/min (43-45)). Blood pressure in the umbilical artery is predicted by the model and in normal pregnancy is 50 mmHg or 6650 Pa (42). Each vessel that is not part of a terminal conduit is assigned a Poiseuille resistance based on its simulated length and diameter, where resistance (R) is defined by

$$R = \frac{8\mu L}{\pi r^4}, \quad (2)$$

with blood viscosity $\mu = 3.36 \times 10^{-6}$ Pa.s, L is the length of the blood vessel and r is its radius. By solving for Poiseuille flow in each vessel element and applying conservation of mass at each vessel bifurcation we can simulate the resistance of the placental vasculature and the distribution of flow within the placental structure as described in Appendix A.3. Heterogeneity in flow is quantified as the coefficient of variation in flow at the capillary pathways (Appendix A.4).

4. Results

4.1. Geometry

The simulated villous structure that best matched literature descriptions of the villous vasculature was comprised of 32,000 seed points, a maximum branch angle of 90° and a fractional distance for vessel growth toward the seed point centre of mass of 0.4. A minimum vessel length was not required. The resultant villous tree extended 15 generations beyond the chorionic arteries (7, 8) with at least 4 generations before a vessel enters the lumped-parameter terminal unit (8). Average pathlength through the villous tree to the level of capillary conduits was 20.43 mm (standard deviation 7.21 mm) which compares to a placental thickness of 20 mm. Noting that branching pathways can be tortuous, this indicates that the geometric algorithm 'fills' the space defined as placenta. The structure had a Strahler branching ratio of 2.65, well within the range of 2.19-2.83 calculated from literature data. Mean branch angles through the placental vasculature are consistent with estimates of branch angles in the periphery of villous trees. However, it should be noted that both measured and generated branch angles cover a wide range. Statistics regarding the branching structure of the model vasculature are given in Table 2. The choice of 32,000 seed points was not the only choice to give a reasonable fit to the prescribed data regarding number of branching

generations and branching ratio. Appropriate fits spanned approximately 3000 data points on either side of the chosen value. Simulating perfusion in the generated tree resulted in a prediction of umbilical artery pressure of 50.86 mmHg (6764.7 Pa). Taking trees generated with more or fewer data points at the extremes this range resulted in predictions of placenta gave a range of umbilical artery pressures of 47.13-51.92 mmHg and the final value of 32,000 seed points was chosen to sit close to the middle of this range at a normal umbilical artery pressure.

<INSERT TABLE 2 HERE>

The chorionic arteries, in accordance with literature descriptions is mostly dichotomous in structure with an average daughter to mother diameter ratio of 0.79, which is comparable to an existing quantitative description with ratios ranging from 0.76-0.8 (4). In comparison the generated chorionic tree with a non-central cord insertion is more asymmetric, with long, higher calibre vessels feeding the periphery far from cord insertion, and vessels feeding villous trees near the cord insertion being small in calibre, as shown in Figure 3c. The case of non-central cord insertion the chorionic plate itself has a larger mean angle for minor pathways (72^{o} compared with 65^{o}), and a larger Strahler branching ratio so more asymmetry than the case of central cord insertion (2.58 compared with 2.47). There were however no significant differences between branching properties of the placental vasculature once the generated villous trees had been incorporated into calculations. There were no significant differences between branching properties of the ellipsoidal placental shape and the spheroidal placental shape.

4.2 Parallel Capillary Connections

The average number of parallel capillary connections per mature intermediate villus is estimated to be approximately 6 (7). A single terminal unit with 3 generations of capillary connections is predicted by our model to have a resistance of 1.9×10^{6} Pa.s/mm^{3}. This is equivalent to a single vessel, having the same diameter as an intermediate villous artery but 9.4 mm long. Remembering that the combined capillary length associated with each intermediate villous artery is18 mm and that our terminal units cover 3 generations, this allows significant additional capillary volume whilst minimising resistance. Figure 5 shows effective length required to represent an increasing number of parallel capillary connections per intermediate villous artery with dimensions as seen in the placenta as an indication of resistance. It is clear that the parallel capillary convolutes present in the placenta allow it to carry the maximum volume of blood to the gas exchange region of the placenta and if in pathological pregnancies capillary connections are missing or redundant as suggested in morphological studies (3, 40), this could have a significant impact on the resistance of the feto-placental vasculature.

<INSERT FIGURE 5 HERE>

4.3. Perfusion simulations

Baseline simulations of perfusion in the spheroidal 'average' placental geometry result in predictions of feto-placental vascular resistance that are consistent with literature estimates of feto-placental haemodynamics. As mentioned previously, the boundary conditions employed result in predictions of umbilical artery blood pressure of 50.86 mmHg (6764.7 Pa), which compares to literature estimates of 50 mmHg (42). Simulations in the placental geometry reflecting non-central cord insertion result in similar predictions of umbilical artery pressure 50.28 mmHg (6687.2 Pa) compared with to the case of central cord insertion, but flow at the capillary level in this case is more heterogeneous in the case of non-central cord insertion. The variability in flow in the case of central cord insertion is illustrated in Figure 6. The

coefficient of variation in capillary convolute blood flow is predicted to be 19.4% with central cord insertion compared with 23.3% with non-central cord insertion with non-central cord insertion. This indicates that the placenta is not less efficient at carrying fetal blood with non-central cord insertion, but if changes in flow heterogeneity are significant to oxygen exchange efficiency there may be implications for the placenta. With an ellipsoidal placental shape the model predicted only minor differences in placental resistance and capillary flow heterogeneity when compared with the spheroidal placenta with an umbilical artery blood pressure of 50.65 mmHg (6793.7 Pa) and a coefficient of variation of 19.7%.

<INSERT FIGURE 6 HERE>

To assess the importance of placental capillary connections in determining placental vascular resistance, we resimulated placental perfusion with the assumed number of parallel capillary connections from each intermediate villous varied from 3 to 10. This increases the effective resistance of the micro-vasculature significantly. Predictions of umbilical artery pressure with reduced capillary pressures rose from 50.86 mmHg (6764.7 Pa) at the baseline state to 60.45 mmHg (8039.6 Pa) with just 3 connections showing that pathology in the placental microvasculature (or capillary pruning) has a significant effect on placental function. Increasing the number of capillary connections has a smaller effect on umbilical artery pressure, and increasing the number of parallel capillary pathways to 10 results in a decrease in umbilical artery pressure to 43.20 mmHg (5475.5 Pa) due to a non-linear effect of adding capillary pathways on the resistance of the lumped-parameter model. Figure 7 shows the non-linear nature of the effect of increasing and decreasing numbers of capillary connections on predictions of umbilical artery pressure. When the number of capillary connections is reduced to 3, capillary flow heterogeneity decreases significantly to a coefficient of variation of 11.4%. A significant increase in capillary flow heterogeneity is predicted in the case of 10 capillary connections with a coefficient of variation of 26.1%.

<INSERT FIGURE 7 HERE>

4.4 Model sensitivity to vessel dimensions

Anatomical data regarding the structure of the placental vasculature is not uniformly obtained using the same techniques and is more complete in describing large arteries than small arteries and veins. Therefore, an assessment was made of the model sensitivity to the calibre of small arteries, capillaries, and veins. First the effect of increasing or reducing the calibre of the intermediate villous vessels and terminal convolutes was assessed, and then the effect of altering venous calibre.

Decreasing the calibre of capillary convolutes had a more significant impact on system resistance than increasing their calibre as the resistance of a vessel is proportional to the reciprocal of the fourth power of radius (so very small vessel radii have a significant increase in resistance). Figure 8 shows the effect of increasing and decreasing intermediate vessel and capillary radius together and separately affects predicted system resistance. Capillary convolute radius has the greatest effect on the resistance of the system as a whole as the placental capillaries comprise a large number of small vessels. A 10% increase in capillary convolute radius decreases predicted feto-placental radius by 12%, and increase the heterogeneity in capillary flow to a coefficient of variation of 24.4%. A 10% decrease in capillary convolute radius conversely increases predicted feto-placental radius by 17%, and decreases the heterogeneity in capillary flow slightly from baseline to a coefficient of variation of 19.2%.

<INSERT FIGURE 8 HERE>

The effect of venous calibre on total resistance is approximately proportional to the increase or decrease in calibre. Increasing the radius of all veins by 10% resulted in a predicted decrease in feto-placental resistance of 9% and a change in coefficient of variation to 22.5%. A decrease in calibre of all veins by 10% resulted in a predicted increase in feto-placental resistance of 11% and a change in coefficient of variation of 16.7%.

Discussion

In this study we have presented an anatomically based geometric model of the term feto-placental vasculature, which includes key geometric features of the vasculature across spatial scales from the umbilical cord insertion to the placental microvasculature. While computational models of the feto-placental vasculature typically 'zoom in' on a region of the vasculature such as the chorionic plate, or assume a simple geometric structure for the whole placenta, our model attempts, for the first time, to incorporate descriptions of feto-placental structure across spatial scales to provide a representative anatomically based, whole organ description of function. This model provides a basis for assessing the impact of placental size and shape on efficiency, and it can be individualised or modified to incorporate new knowledge regarding placental structure and function from 3D imaging technologies, which are emerging to provide an increasing resolution for imaging structure and function in the placenta *in vivo* and *ex vivo* (40, 46-48).

There is much discussion in the literature comparing placental shape and chorionic vessel structure to placental efficiency (16, 18, 21). While there appears to be some influence of placental shape and structure on efficiency, these features are rarely linked to severe pathology except in extreme cases (18). As the *in vivo* placenta is inaccessible to direct measurement, anatomically based *in silico* models of the placental vasculature provide an opportunity to assess proposed hypotheses regarding structure-function relationships in the placenta. Our model predicts that normal variation in placental ellipticity is unlikely to affect vascular resistance or heterogeneity of flow within the vasculature. However, while the asymmetry in vascular structure bought upon by non-central cord insertion is not predicted to affect placental resistance, it is predicted to influence flow heterogeneity in placental capillaries. This is likely due to the combined influence of long pathways to the periphery of the placenta far from cord insertion. Computational models of oxygen exchange in the placenta suggest that a good balance between maternal and fetal blood flow rates is a key factor in gas exchange efficiency (49) and increases in flow heterogeneity may influence this balance. Future development of multi-scale models of gas exchange in the placenta, including asymmetry in vessel structure may be the key in determining whether any changes in placental efficiency due to asymmetric vascular structure are significant enough to influence development.

Simulations assessing the effect of placental shape and cord insertion were conducted assuming that the placental micro-vascular structure is the same between placentas. The smallest placental capillaries have the highest individual resistance and so are large contributors to feto-placental resistance. Our model predicted that the number of parallel capillary pathways significantly influences the resistance of the placenta. Studies have shown that sparser capillary networks (1, 2) are found in several pregnancy complications such as pre-eclampsia, fetal growth restriction, and cases of pregestational maternal diabetes. These same conditions are often associated with abnormal umbilical Doppler, and our model supports the hypothesis that placental pruning, or fewer small placental vessels is related to abnormal umbilical feto-placental resistance, and hence abnormal Doppler indices. Giles et al. (50) compared the density of small villous blood vessels to umbilical artery flow velocity waveforms and found high Doppler indicated resistance to relate to low vessel counts. On the other hand, increased capillary branching is associated with maternal anaemia, maternal smoking, and late onset pre-eclampsia are associated with excessive branching of capillaries

(2, 51). These conditions are associated with excessive placental weight, but often-normal fetal Doppler indices (2). In the case of excessive capillary branching our model predicts a decrease in overall feto-placental resistance, but this is far less marked than the increase observed with sparse capillary branching. As feto-placental resistance is related to Doppler indices, particularly the resistance index, it may be that this small change in resistance is not easily detectable, or that other changes in placental morphology also contribute to feto-placental resistance in these conditions.

Both excessive and sparse capillary branching are associated with changes in flow heterogeneity in our model. Flow distribution and heterogeneity in the placenta has been assessed in diabetic pregnancies and growth restricted pregnancies using MRI (46, 52), although this method allows only visualisation of a combination of feto-placental and utero-placental flow, so is not currently directly comparable to the model. However, consideration of both utero-placental and feto-placental contributions to flow heterogeneity should be an important consideration in the future to allow direct comparison to this type of imaging study. Our model is sensitive to the calibre of capillary vessels both in terms of flow resistance and flow heterogeneity. Assessments of capillary calibre in several pregnancy pathologies have not shown a consistent change in the size of capillaries in pathology (51), suggesting there may be variability within a cohort. MRI and Doppler imaging studies combined with histology, such as that of Giles et al. (50), provide an ideal way to test the flow resistance and heterogeneity metrics predicted by our multiscale model against experimental measures of similar quantities in the long term, and allow variation in response to a pathology between individuals to be considered, as imaging can be linked to morphology. Although our multi-scale model includes the terminal unit resistance as a single resistor, we incorporate some key structural features of the placental micro-vasculature in calculation of this resistance. Additional complexity, such as redundant capillary connections (2, 3), could feasibly be incorporated into this framework, particularly as new quantitative imaging data at this spatial scale becomes available.

This model is not restricted to consideration of the *in-vivo* placenta. *Ex-vivo* placental perfusion systems are often used to assess placental transport function (53). These systems are typically perfused with a steady flow, making our model resistance directly comparable to the resistance of the system, if measured. The *ex-vivo* placenta can also be imaged using MRI, or detailed morphological studies conducted. With an extended computational model to account for placental transport, similar to the type of model employed by Hill et al. (31, 49) or Sengers et al.(32), the relationship between structure and function predicted by the model could not only be tested, but could be incorporated into studies of placental transport and drug delivery within these systems. This would provide a powerful tool for predicting how placental transport might respond to different perfusion conditions or pathologies, and could provide important predictions to translate the behaviours of an *ex-vivo* system to *in-vivo* placental transport.

We include detailed descriptions of the branching structure of the placental vasculature in our model such as branching ratios and asymmetry indices, which are typically reported in studies of other biological branching networks (54, 55). Not all of these indices have been reported in the placenta, particularly the human placenta, as accessibility of tissue has limited detailed studies that have been possible in other organs. However, recent studies have employed high-resolution 3D imaging to begin to quantitatively assess villus structure (47) These methodologies will likely be applied to the villous vasculature in coming years. The diversity of techniques used in anatomical studies in the literature, with some information obtained from *ex vivo* casts, or 2D tissue sections, limits our knowledge of placental anatomy, particularly in the smallest capillary structures. This limits the accuracy of our model. Although our model accurately reflects current data regarding the branching villous structure and placental resistance we anticipate that refinements will be possible as more quantitative

structural data becomes available. To address this limitation an analysis of the sensitivity of model results to vessel calibre was undertaken. The analysis suggests that the model is highly sensitive to the definition of capillary calibre and so more accurate descriptions of structure at this scale will be key to improving model accuracy. This model provides a framework for anatomically based modelling of the placenta and can be individualised using morphometric or ultrasound based data on placental shape and large vessel structure, as has been demonstrated effectively in anatomically based models of other organs (33). Combined with models of uterine perfusion we anticipate that this model framework could also be used to assess placental flow heterogeneity and its changes in pathology as observed in MRI studies (46). It also lends itself to adaption for simulation of function in early pregnancy, where capillary beds are not completely formed. It is clear from simulation results that capillary structure is a key contributor to placental resistance and simulation of early changes in this structure may provide indications of subtle changes in placental efficiency in the early stages of pathology.

Model limitations and possible extensions

A steady-state model of perfusion was presented in our anatomically based placenta geometry, whereas blood flow in the placenta is pulsatile and it is changes in this pulsatile nature that are most useful for identifying placental abnormalities (10). Feto-placental resistance can be indirectly related to Doppler ultrasound indices, including the resistivity index and the pulsatility index, however pulsatile flow simulations would strengthen model predictions by allowing a direct comparison. While it is feasible to solve for Navier-Stokes flow in small numbers of vessels, or to solve one-dimensional simplifications to the Navier-Stokes equations over several generations of blood vessels, computational time is an issue in large anatomically based geometries. To achieve a useful model a balance between computational time and accuracy of fluid dynamics equations must be met. We have recently shown that solving for wave propagation in anatomical geometries of a similar size to the one proposed here is feasible with manageable computational times (56), and anticipate that these techniques will provide an avenue to simulate key measures of pulsatile function in the whole placenta and to allow variations in placental structure to be directly linked to clinical indices, and in particular Doppler ultrasound waveforms.

Blood is assumed to be a Newtonian fluid throughout, which is assumed to be valid where vessel calibre far exceeds the dimensions of the blood cells within a vessel. In the smallest capillary vessels this assumption may not hold. The Fahraeus-Lindqvist effect may play a role in the smallest blood vessels, in which case the effective viscosity of blood is decreased in the smallest placental blood vessels. In other models of this type, the viscosity of blood is assumed to vary with vessel radius, either in a linear manner (41), or based on empirical formulae as a function of vessel radius and hematocrit (57). This reduction in viscosity would reduce resistance of the smallest vessels and potentially influence the magnitude of pressure drops predicted in Figure 7.

In our model we assume each blood vessel to be a cylindrical tube. While blood vessels often have close to circular cross-sections, vascular profiles often deviate from this norm. This is likely to be particularly true in placental capillary convolutes which are often easily dilated and may take on a more elliptical cross section. Some previous studies have attempted to assess the importance of asymmetric vascular profiles at this level in other organs by assuming elliptical cross-sections and amending vessel resistance accordingly (13). With morphometric data on vessel cross-sections, this kind of asymmetry in flow would be an important extension to implement in a model of this type. The model also neglects the distensibility of placental blood vessels, which potentially acts to reduce resistance and could to mitigate changes in pressure at increased flow rates. Alternatively as many morphometric studies, including data sources used to parameterise our model, are based on casting, which is

often conducted at high inflation pressures, neglecting vessel distensibility could result in an underestimate of placental resistance. There is limited data on placental vessel distensibility. However, vessel compliance should be key considerations in future studies. Longer term, the influence of vasoactive mediators should be incorporated into models. There are several active control methods that control resistance in the feto-placental vasculature, and important vasoactive mediators appear to vary between chorionic and villous vessels (58). Modelling the interaction between feto-placental blood flow distribution and vasoactive function could potentially increase understanding of the evolution of pathology, as the vasculature develops and remodels.

Previous models of placental function have used simplified geometrical descriptions of the placenta, or placental subunits (30-32, 49). In this type of model the savings made in neglecting geometrical complexity allows for either a simple and quick to use model, or detailed consideration of aspects of function (such as the kinetics of transfer processes). The complexity required from a model depends on the question that is being asked of the system. The model proposed here allows assessment of the contributions of the structure of the placental vasculature that have been proposed in the literature (specifically shape and branching structure) to be assessed in a unified framework. Compartmental models, on the other hand, can be highly predictive in providing an averaged, whole organ description of function. An appropriate multi-scale model of the system must take into account levels of complexity across spatial scales, and remain simple enough to be computationally tractable. Therefore, there is always a trade-off between the level of complexity that can be included in a model, while adequately addressing the biological question at hand.

Conclusions:

Multi-scale modelling is critical for understanding the evolution of placental structure-function relationships. Although individual scale models set up with the available information are useful for answering particular questions, there are still gaps in our knowledge about how each aspect of the placenta system interacts with each other. Unlike the case of other organs, these gaps in knowledge are not easily bridged using animal models due to the wide structural diversity of placenta amongst species (23) and hence studies based on animal models are typically unsuitable or have limited applicability for extrapolation to the human placenta. The multiscale approach adopted in this paper demonstrates how knowledge about different individual scale can be pieced together using a computational model and shows how the model is applied to bridge the gaps in available data. For example, the model provides a mechanism to link *ex vivo* imaging of placental micro-structure to whole organ function. The postulations derived from this model provide useful tools for explaining structure and function relationship in normal and pathological placentas. We anticipate that development of multi-scale models of placental and uterine perfusion, as well as oxygen and nutrient exchange, combined with quantitative assessments of the placental structure across spatial scales will provide key insights into placental physiology through gestation.

Acknowledgements

The authors would like to acknowledge a Royal Society of New Zealand Marsden grant number UOA-13-032. Dr A Clark is supported by an Aotearoa Foundation Postdoctoral Fellowship and Mrs R Saghian is supported by a Gravida (National Centre for Growth and Development) postgraduate scholarship.

A. Appendices

A.1 Finite element mesh

To construct a finite element mesh to represent the placental shape, first a cloud of data points was created to represent the outer boundary of the placenta. Although placental shape in this study represents an averaged, well-defined shape, if the placental shape were to be obtained from imaging studies this methodology would allow for a geometry to be created. In this study the outer shape of the placenta was represented by an ellipsoid using the formula

$$\frac{x^2}{r_{maj}^{\,2}} + \frac{y^2}{r_{\min}^{\,2}} + \frac{z^2}{\tau^2} = 1, \quad \text{(A.1)}$$

where r_{maj}, r_{min}, and τ are semi-axis lengths for the ellipsoid, representing the major axis radius, the minor axis radius and half the placental thickness respectively. In the case that the placenta is an oblate spheroid $r_{maj}=r_{min}$. A cloud of data points satisfying equation (A.1) was generated using a perl script.

An initial trilinear finite element mesh was constructed to represent a generic placental shape and a cubic Hermite mesh was fitted to the generated data cloud. This generic mesh consisted of 17 nodes, with 8 nodes equispaced along the surface of the data clout at z=0, a further 6 nodes equispaced along the surface *y=0*, and the remaining nodes sitting along the centre-line of the volume (*z=0* and *y=0*). The data cloud and the template mesh were imported into the finite element package CMISS (http://www.cmiss.org) for fitting with the visualisation tool CMGUI (http://www.cmiss.org/cmgui) used to manually adjust the fit between iterations. The methodology for fitting a cubic Hermite mesh to the data cloud is given in Fernandez et al. (1). In brief, the volume elements of the mesh are decomposed into faces and these faces are treated as area elements. The 'data error' is determined by summing the square of the distances between each data point and its projection onto the external faces of the mesh. The face objective function is defined as the data error plus a Sobolev smoothing term, and this objective function is differentiated with respect to each face parameter (nodal value, three first-order derivatives in the *x*-, *y*-, and *z*-directions, three second-order or cross-derivatives and a third-order derivative) and the resulting expression equated to zero to provide new face parameters and scale factors for the mesh. The process of projecting data onto the external faces of the mesh and updating face parameters and scale factors is repeated until the root mean square data error is less than a prescribed tolerance or a maximum number of iterations. In this case fits were achieved with a root mean squared (RMS) error of less than 1mm.

A.2. Seed data points and tree growing algorithms

Chorionic vessels: To create seed points toward which to grow chorionic vessels the finite element mesh representing placental shape was imported into CMGUI. The faces on one side of the placenta (the chorionic surface) were selected and a Poisson distributed seed point cloud was generated over these surfaces using inbuilt CMGUI functionality. The resulting data points were imported into MeshLab (http://meshlab.sourceforge.net) and their density reduced using Poisson disk sampling. The resulting trimmed data cloud consists of a user-defined number of approximately equispaced data points.

Villous trees: Seed point data was generated to fill the volume mesh defining the shape of the placenta using the CMISS software. The algorithm employed defines a seed point density and generates an equispaced array of seed points that fill the shape described by the finite element mesh. The density of seed points was iteratively altered and the growing algorithm (described below) re-implemented to achieve the geometric parameters described in the main text of the article.

Tree growing algorithm: The tree growing algorithm used was developed by Wang et al. (2) and extended to 3D volumes by Tawhai et al (3). A schematic illustration of the area-filling

branching algorithm of Wang et al. (2) is given in Figure 2. The algorithm proceeds are follows:

1. Seed data points are defined over the area or volume of interest.

2. 'Stem' arteries are placed from which trees emerge. In the case of the chorionic vessels this is the umbilical insertion, and in the case of the villous trees it is the terminal points of the generated chorionic vessels

3. The seed points are split into two groups defined in 2D by the line between the starting point of the growing and the centre of mass of the seed points, and in 3D the plane defined by this line and the vector in the direction of the parent branch and the centre of mass of the seed points was used to split the seed points.

4. The centre of mass of the two new sub-regions are calculated and new branches are grown a pre-defined distance from the start point to these two centres of mass.

5. Checks are made to ensure that branching angles and new vessel lengths are within pre-defined limits. If not, the branch angle is reduced, or the vessel is considered to be a terminal vessel and the algorithm is terminated for this group of seed points.

6. Steps 3-5 are repeated with progressively smaller sets of seed points until a minimum branch length is reached or there is only one seed point left in each group.

A.3 Blood flow simulations

Each blood vessel is described in the model by the vector between its start at and end point of the vessel and its radius. The pressure drop (ΔP) across each vessel is described by

$$\Delta P = QR, \quad \text{(A.2)}$$

where Q is the volumetric blood flow rate through the vessel and R is the vessel resistance. The vessel resistance is defined as a Poiseuille resistance (Equation 2), which can be calculated from the geometric description of the vessel tree. At each bifurcation, the flow through the parent vessel (Q_p) divides into two daughter vessels with flow Q_{d1} and Q_{d2}. By applying conservation of mass

$$Q_p = Q_{d1} + Q_{d2}. \quad \text{(A.3)}$$

By assuming a continuity of pressure across each bifurcation we also define the pressure at the outlet of a parent branch to be equal to the pressure at the inlet of its daughters. This gives us a system of unknowns to solve for. That is, flow in each branch and pressure at each bifurcation. By defining boundary conditions of pressure or flow at each inlet or outlet and assuming rigid vessels we can solve a linear system for each of these unknowns and define the flow distribution through the whole geometry.

This approach is taken both in the large asymmetric branching tree and the lumped parameter model representing the intermediate villous vessels and capillary conduits. However, in this lumped parameter model resistance can be calculated for the whole unit by summing resistances using electrical circuit theory similar to the study of Clark et al. (4). Each vessel is

thought of as a resistor which lies in series or in parallel to other resistors in the lumped parameter model. All vessels at the same generation can be thought of as parallel resistors and their total resistance summed in parallel. That is, for a number of resistors with resistance (R_i) in parallel

$$\frac{1}{R} = \sum \frac{1}{R_i} \quad \text{(A.3)}$$

Following this approach we calculate the resistance of each individual generation of vessels and then sum the resistance of each generation of vessels in series (which is the direct sum of each individual resistance).

A.4 Calculating flow heterogeneity

Flow heterogeneity is calculated only at the level of the lumped parameter model. To do this the flow through each lumped parameter unit is recorded and the coefficient of variation, defined as the standard deviation of flow divided by the mean flow, is calculated.

References

1. Teasdale F, Jean-Jaques G. Intrauterine growth retardation: Morphometry of the microvillous membrane of the human placenta. Placenta. 1988;9:47-55.
2. Kingdom J, Huppertz B, Seaward G, Kaufmann P. Development of the placental villous tree and its consequences for fetal growth. Eur J Obstet Gynecol Reprod Biol. 2000;92:35-43.
3. Jirkovská M, Kubínová L, Krekule I, Hach P. Spatial arrangement of fetal placental capillaries in terminal villi: A study using confocal microscopy. Anat Embryol. 1998;197:263-72.
4. Gordon Z, Elad D, Almog R, Hazan Y, Jaffa A, Eytan O. Anthorpometry of fetal vasculature in the chorionic plate. J Anat. 2007;211:698-706.
5. Benirschke K, Kaufmann P. Umbilical Cord and Major Fetal Vessels. Pathology of the Human Placenta: Springer New York; 1990. p. 180-243.
6. Kishore N, Sarkar S. The arterial patterns of placenta. A postpartum radiological study. J Obstet Gynaecol India. 1967;17:9-13.
7. Leiser R, Kosanke G, Kaufmann P. Human placental vascularization. In: Soma H, editor. Placenta: Basic research for clinical application Basel, Germany: Karger; 1991.
8. Kaufmann P, Luckhardt M, Leiser R. Three-dimensional representation of the fetal vessel system in the human placenta. Trophoblast Research. 1988;3:113-37.
9. Kosanke G, Castellucci M, Kaufmann P, Mironov V. Branching patterns of human placental villous trees: Perspectives of topological analysis. Placenta. 1993;14:591-604.
10. Kingdom J, Burrell S, Kaufmann P. Pathology and clinical implications of abnormal umbilical artery Doppler waveforms. Ultrasound Obstet Gynecol. 1997;9:271-87.
11. De Smedt M, Visser G, Meijboom E. Fetal cardiac output estimated by Doppler echocardiography during mid and late gestation. Am J Cardiol. 1987;60(4):338-42.
12. Giles W, Trudinger B, Baird P. Fetal umbilical artery flow velocity waveforms and placental resistance: Pathological correlation. Brit J Obstet Gynaecol. 1985;92:31-8.

13. Barker D. The long term outcome of retarded fetal growth. Clin Obstet Gynecol. 1997;40(4):853-63.
14. Kaplan C. Gross pathology of the placenta: Weight, shape, size colour. J Clin Pathol. 2008;61:1285-95.
15. Benirschke K, Kaufmann P. Macroscopic Features of the Delivered Placenta. Pathology of the Human Placenta: Springer New York; 1990. p. 13-5.
16. Pathak S, Hook E, Hackett G, Murdoch E, Seibert N, Jessop F, Lees C. Cord Coiling, umbilical cord insertion and placental shape in an unselected cohort delivering at term: Relationship with common obstetric outcomes. Placenta. 2010;31:963-8.
17. De Paula C, Ruano R, Campos J, Zuqaib M. Placental volumes measured by 3-dimensional ultrasonography in normal pregnancies from 12 to 40 weeks gestation. J Ultrasound Med. 2008;27:1583-90.
18. Salafia C, Yampolsky M, Misra D, Shlakhter O, Haas D, Eucker B, Thorp J. Placental surface shape, function, and effects of maternal and fetal vascular pathology. Placenta. 2010;31:958-62.
19. Cotter S, Klika V, Kimpton L, Collins S, Heazell A. A stochastic model for early placental development. J R Soc Interface. 2014;11:20140149.
20. Collins S, Stevenson G, Noble J, Impey L. Rapid calculation of standardized placental volume at 11-13 weeks and the prediction of small for gestational age babies. Ultrasound Med Biol. 2013;39(2):253-60.
21. Winder N, Krishnaveni G, Veena S, Hill J, Karat C, Thornburg K, Fall D, Barker D. Mother's lifetime nutrition and the size, shape and efficiency of the placenta. Placenta. 2011;32:806-10.
22. Heifetz S. The umbilical cord: Obstetrically important lesions. Clin Obstet Gynecol. 1996;39(2):571-87.
23. Carter A. Animal models of human placentation - A review. Pacenta. 2007;28 Supplement:S41-S7.
24. James J, Carter A, Chamley L. Human placentation from nidation to 5 weeks of gestation. Part II: Tools to model the crucial first days. Placenta. 2012;33(5):335-42.
25. Gordon Z, Eytan O, Jaffa A, Elad D. Fetal blood flow in branching models of the chorionic arterial vasculature. Ann NY Acad Sci. 2007;1101:250-65.
26. Franke V, Parker K, Wee L, Fisk N, Sherwin S. Time domain computational modelling of 1D arterial networks in monochorionic placentas. ESAIM-Math Model Num. 2003;37(4):557-80.
27. Yang J, Yu L, Rennie M, Sled J, Henkelman R. Comparative structural and hemodynamic analysis of vascular trees. Am J Physiol Heart Circ Physiol. 2010;298:H1249-H59.
28. Guiot C, Pianta P, Todros T. Modelling the feto-placental circulation: 1. A distributed network predicting umbilical haemodynamics throughout pregnancy. Ultrasound Med Biol. 1992;18:535-44.
29. Todros T, Guiot C, Piantà P. Modelling the feto-placental circulation: 2. A continuous approach to explain normal and abnormal flow velocity waveforms in the umbilidal arteries. Ultrasound Med Biol. 1992;18:545-51.
30. Chernyavsky I, Jensen O, Leach L. A mathematical model of intervillous blood flow in the human placentone. Placenta. 2010;31:44-52.
31. Hill E, Power G, Longo L. A mathematical model of carbon dioxide transfer in the placenta and its interaction with oxygen. Am J Physiol. 1973;224(2):283-99.

32. Sengers B, Please C, Lewis R. Computational modelling of amino acid transfer interactions in the placenta. Exp Physiol. 2010;95(7):829-40.
33. Clark A, Tawhai M, Hoffman E, Burrowes K. The interdependent contributions of gravitational and structural features to perfusion distribution in a multiscale model of the pulmonary circulation. J Appl Physiol. 2011;110(4):943-55.
34. Boyd P. Quantitative structure of the normal human placenta from 10 weeks gestation to term. Early Hum Dev. 1984;9:297-307.
35. Fernandez J, Mithrarathe P, Thrupp S, Tawhai M, Hunter P. Anatomically based geometric modelling of the musculo-skeletal system and other organs. Biomech Model Mechanobiol. 2004;2(3):139-55.
36. Patel J, Patel B, Dave R, Ram S, Bhojak N, Desai J. A study of placental vascular pattern by corrosive cast in the Gujuarat region. Natl J Integr Res Med. 2014;5(1):64-71.
37. Mu J, Kanzaki T, Tomimatsu T, Fukuda H, Fujii E, Fuke S, Wasada K, Takeuchi H, Murata Y. A comparative study of intraplacental villous arteries by latex case model in vitro and color Doppler flow imaging in vivo. J Obstet Gynecol Res. 2001;27(5):297-303.
38. Wang C, Bassingthwaighte J, Weissman L. Bifurcating distributative system using Monte Carlo method. Math Comput Modeling. 1992;16(3):91-8.
39. Tawhai M, Pullan A, Hunter P. Generation of an anatomically based three-dimensional model of the conducting airways. Ann Biomed Eng. 2000;28:793-802.
40. Jirkovská M, Kubínová L, Janáček J, Moravcová M, Krejči V, Karen P. Topological properties and spatial organization of vollous capillaries in normal and diabetic placentas. J Vasc Res. 2001;39:268-78.
41. Clark A, Burrowes K, Tawhai M. Contribution of serial and parallel microperfusion to spatial variability in pulmonary inter- and intra-acinar blood flow. J Appl Physiol. 2010;108:1116-26.
42. Wang Y, Zhao S. Placental Blood Circulation. Vascular Biology of the Placenta. San Rafael (CA): Morgan & Claypool Life Sciences; 2010.
43. Mielke G, Benda N. Cardiac output and central distribution of blood flow in the human placenta. Circulation. 2001;103:1662-8.
44. Kiserud T, Ebbing C, Kessler J, Rasmussen S. Fetal cardiac output, distribution to the placenta and impact of placental compromise. Ultrasound Obstet Gynecol. 2006;28:126-36.
45. Kiserud T, Acharya G. The fetal circulation. Prenat Diagn 2004;24:1049-59.
46. Moore R, Strachan B, Tyler D, Duncan K, Baker P, Worthington B, Johnson I, Gowland P. In utero perfusing fraction maps in normal and growth restricted pregnancy measured using IVIM echo-planar MRI. Placenta. 2000;21(7):726-32.
47. Haeussner E, Buehlmeyer A, Schmitz C, von Koch F, Frank H-G. Novel 3D microscopic analysis of human placental villous trees reveals unexpected significance of branching angles. Scientific Reports. 2014;4:6192.
48. Collins S, Stevenson G, Noble J, Impey L. Developmental changes in spiral artery blood flow in the human placenta observed with colour doppler ultrasonography. Placenta. 2012;33:782-7.
49. Hill E, Power G, Longo L. A mathematical model of placental O2 transfer with consideration of hemoglobin rates. Am J Physiol. 1972;222:721-9.
50. Giles W, Trudinger B, Baird P. Fetal umbilical artery flow velocity waveforms and placental resistance: pathological correlation. Br J Obstet Gynaecol. 1985;92(1):31-8.

51. Mayhew T, Charnock-Jones D, Kaufmann P. Aspects of human fetoplacental vasculogenesis and angiogenesis. III. Changes in complicated pregnancies. Placenta. 2004;25(2-3):127-39.
52. Deshpande R, Anblagan D, Jones N, Costigan C, Raine-Fenning N, Mansell P, Leach L, Gowland P, Bugg G. MRI for the assessment of placental blood flow in diabetic pregnancies. Arch Dis Child Fetal Neonatal Ed. 2011;96:Fa105-Fa6.
53. Hutson J, Garcia-Bournissen F, Davis A, Koren G. The Human Placental Perfusion Model: A Systematic Review and Development of a Model to Predict In Vivo Transfer of Therapeutic Drugs. Clin Pharmacol Ther. 2011;90:67-76.
54. Cassot F, Lauwers F, Fouard C, Prohaska S, Lauwers-Cances V. A novel three-dimensional computer-assisted method for a quantitative study of microvascular networks of the human cerebral cortex. Microcirculation. 2006;13:1-18.
55. Horsfield K. Quantitative morphology and structure: Functional correlations in the lung. Monogr Pathol. 1978;19(151-159).
56. Postles A, Clark A, Tawhai M, editors. Dynamic blood flow and wall shear stress in pulmonary hypertensive disease. Proceedings of the 36th Annual International Conference of the IEEE EMBC; 2014.
57. Kiani M, Hudetz A. A semi-emperical model of apparent blood viscosity as a function of vessel diameter and discharge hematocrit. Biorheology. 1990;28(1-2):65-73.
58. Myatt L. Current topic: Control of vascular resistance in the human placenta. Placenta. 1992;13:329-41.

Table and Figure captions:

Table 1: Key geometric and model parameters

Parameter name where defined in text	Description	Reference	Value
V	Placental volume	(16)	428 cm^3
τ	Placental thickness	(5)	2.48 cm
r	Placental radius	-	Variable depending on shape
	Number of vessels supplying villous trees	(4,32)	70
	Radius of umbilical artery	(4,8)	2 mm
	Radius of umbilical vein	(4,8,17)	4 mm
	Diameter of mature intermediate villous	(7)	0.03 mm
	Length of mature intermediate villous	(7)	1.5 mm
	Diameter of terminal capillary	(7)	0.0144 mm
	Length of terminal capillary	(7)	3 mm
	Diameter of arteries feeding terminal conduits	(7)	0.03 mm
	Diameter of placental veins	(17)	Twice arterial

			diameter
	Strahler diameter ratio	-	1.53
μ	Viscosity of blood	(29)	3.36×10^{-6} Pa s
	Umbilical blood flow rate	(39-41)	250 ml/min

1

2 **Table 2:** Key metrics describing generated branching placental trees. Standard deviations
3 (s.d.) are given in brackets where applicable.

Metric	**Generated Value (s.d.)**	**Literature value when available (Reference)**
Maximum generations distal to chorionic plate	15	15 (7,8)
Mean number of generations (including chorionic plate)	18.41	-
Mean number of generations (excluding chorionic plate)	10.41	-
Mean branching angle (s.d.)	51.04^o (33.91^o)	Only measured in terminal branches, with wide range 40-70^o in most normal placentas. (43)
Major/minor branching angles	50.76^o / 51.33^o	
Length to diameter ratio (s. d.)	15.87 (8.21)	
Diameter/diameter of parent (s.d.)	0.79 (0.12)	Chorionic vessels only 0.76-0.80 (4)
Strahler branching ratio	2.65	2.19-2.83 (9)
Average diameter of branches entering villous space (approximately Strahler order 8)	0.70 mm	0.7 mm (7)
Average diameter of branches feeding terminal units (Strahler order 1)	0.03 mm	0.03 mm (7)

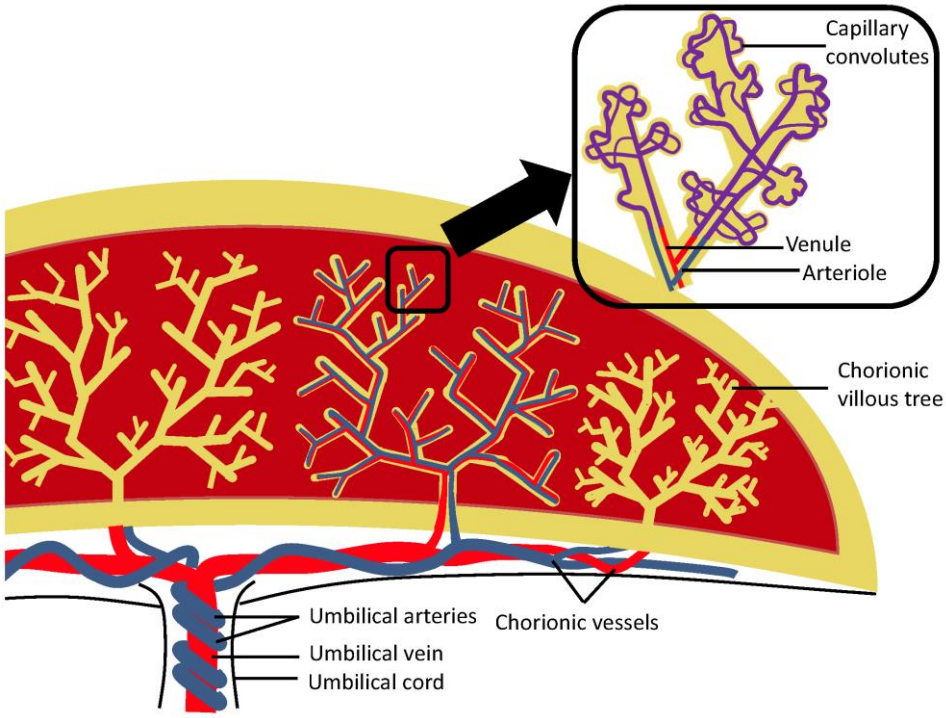

Figure 1: A schematic illustration of the structure of the placental vasculature. Deoxygenated blood is delivered to the placenta via two umbilical arteries. These arteries branch into large chorionic vessels which feed 60-100 individual villous trees. The villous trees themselves branch dichotomously for several generations before feeding several parallel capillary conduit pathways, which provide the site for placental gas exchange. Several parallel pathways between arteries and veins in the villous tree are incorporated at the level of the intermediate and terminal villi in the model developed here, as have been observed in cast and imaging based studies. However, for simplicity, only a single artery and vein per villous branch are shown in the figure (inset).

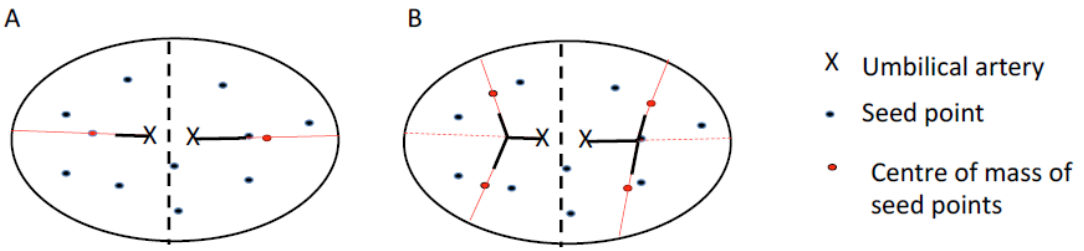

Figure 2: A schematic illustration of the area-filling branching algorithm of Wang et al. (38). Initial placement of the umbilical arteries is assigned and seed points are split into two groups. A. The centre of mass of seed points in each group is calculated and a new artery is grown a prescribed distance toward this centre of mass. B. The collection of seed points is split according to the centrelines of the newly generated arteries, centres of mass for each subregion are recalculated and four new branches generated a fixed distance toward these points. The process is repeated until there is only one seed point left in each group.

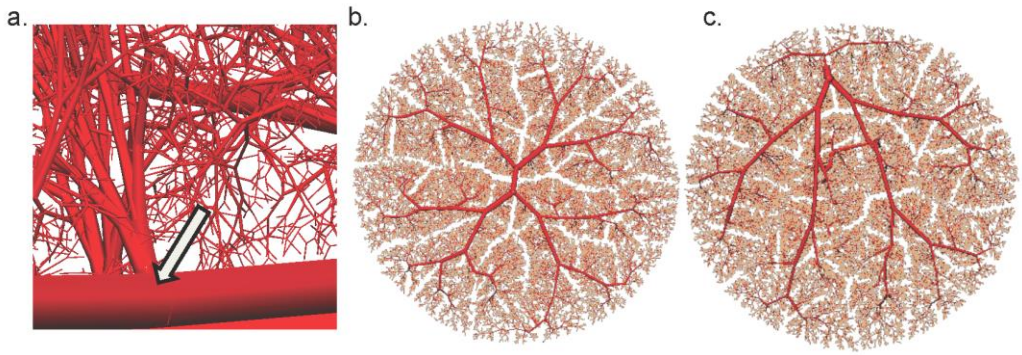

Figure 3: Graphical depictions of the model geometry. (a) A intraplacental vessel which is much smaller in diameter than the main chorionic vessels arising from a chorionic vessel at close to right angles. The largest placental arteries in the case of (b) central and (c) non-central cord insertion, in accordance with previous studies the case with central cord insertion is relatively more symmetric than the case of non-central insertion. Veins and peripheral small arteries and capillaries are not shown.

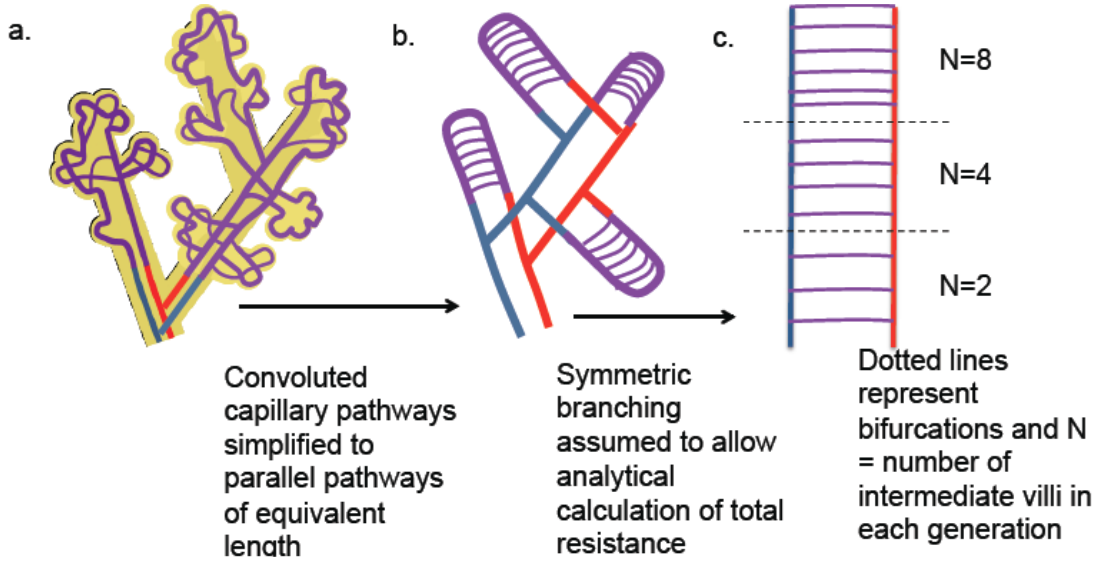

Figure 4: Illustrations of the model description of terminal capillary conduits. (a) In the placenta mature intermediate villus vessels branch and each intermediate villus gives rise to on average 6 terminal convolutes that follow tortuous pathways from artery to vein. (b) we model these terminal convolutes as arising consecutively from intermediate villus arteries and neglect any connections between capillary convolutes. (c) Finally, we assume that intermediate villus arteries branch symmetrically so the number of vessels doubles at each generation. Resistance of the terminal portions of the placental vasculature can then be summed in serial and parallel through the system.

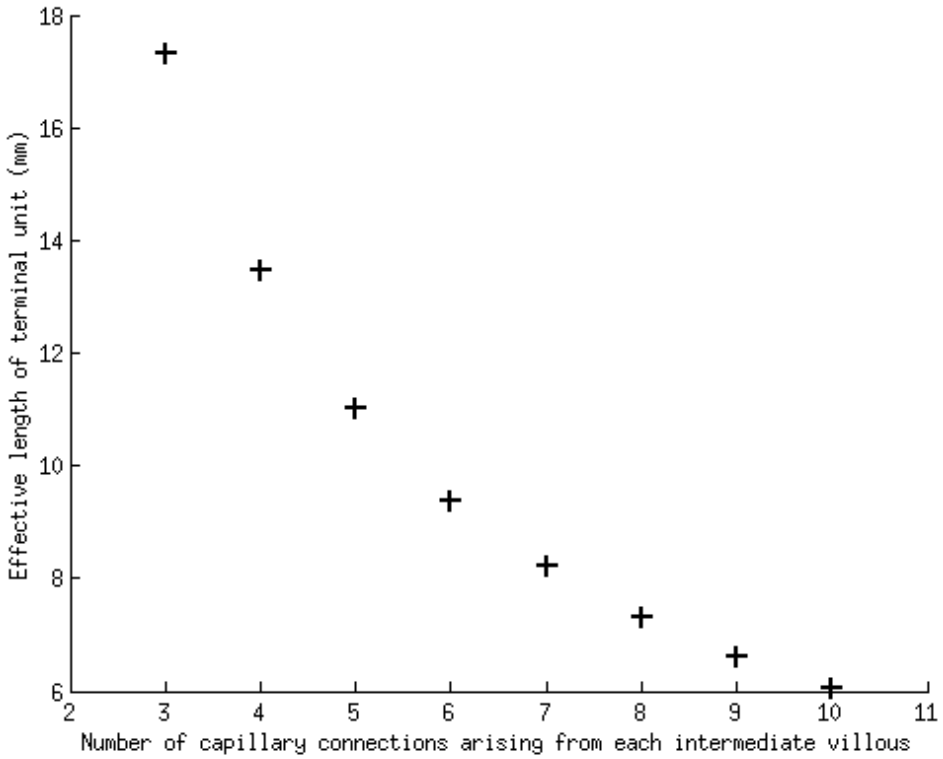

Figure 5: Model simulations of the effective resistance of a terminal unit, expressed as the effective length of a single vessel with the same radius as an intermediate villus, plotted against the number of parallel capillary connections associated with an intermediate villus. The model suggests that parallel capillary connections contribute to maximising the capillary surface area available to gas exchange whilst allowing the resistance of the placental vasculature to stay low.

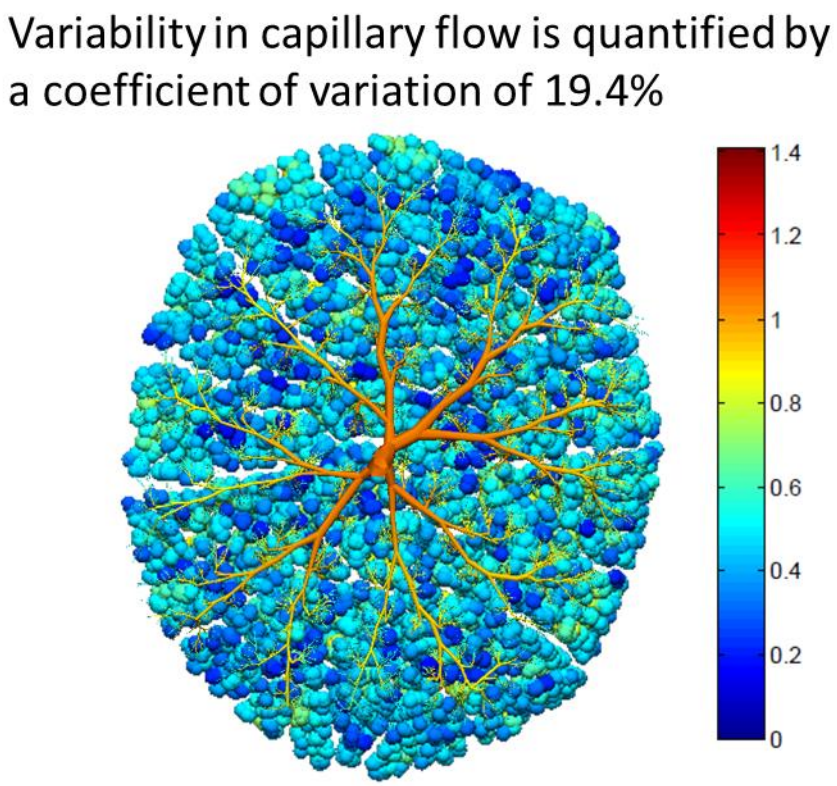

Figure 6: An illustration of model predictions of the heterogeneous distribution of flow to placental capillaries. Each capillary unit is represented as a sphere and the relative flow in each sphere is represented by a linear red-blue colour scale (range X-Y). Large placental arteries are also shown, coloured by predicted blood pressure.

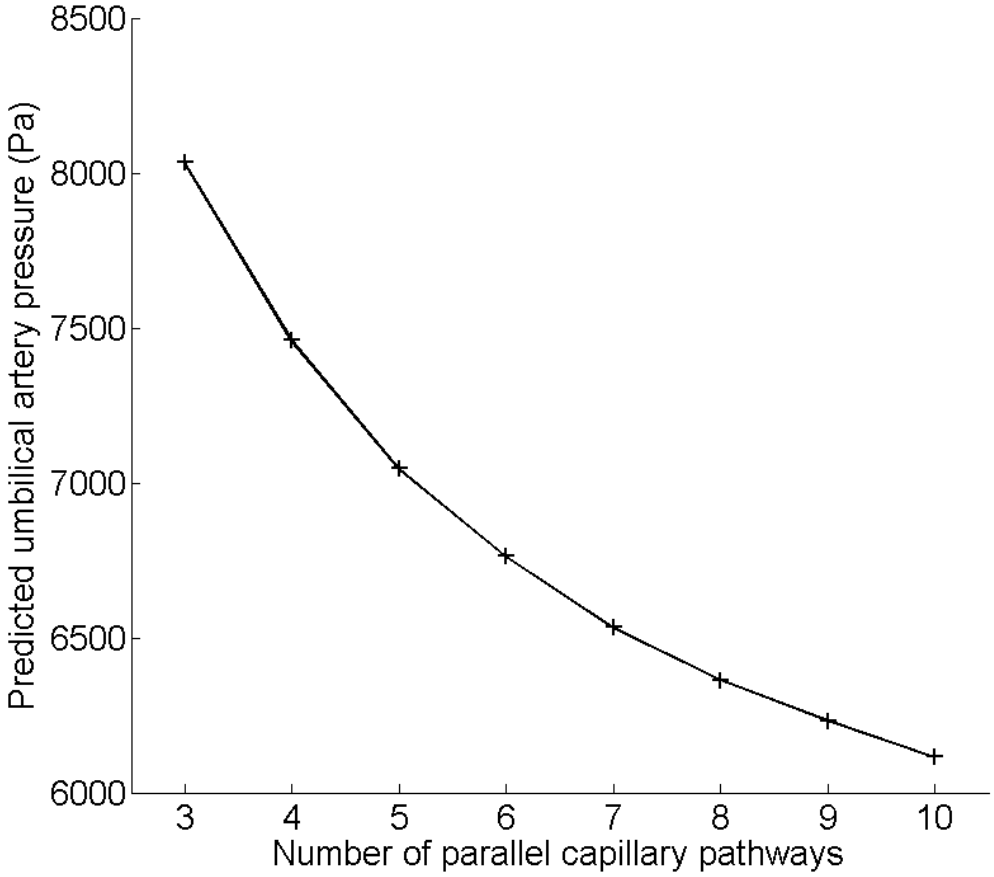

Figure 7: Model predictions of the umbilical artery pressure as a function of the number of parallel capillary connections associated with an intermediate villus. This indicates that in pathological pregnancies with insufficient parallel capillary connections, an increased umbilical artery pressure could put additional strain on the fetal heart.

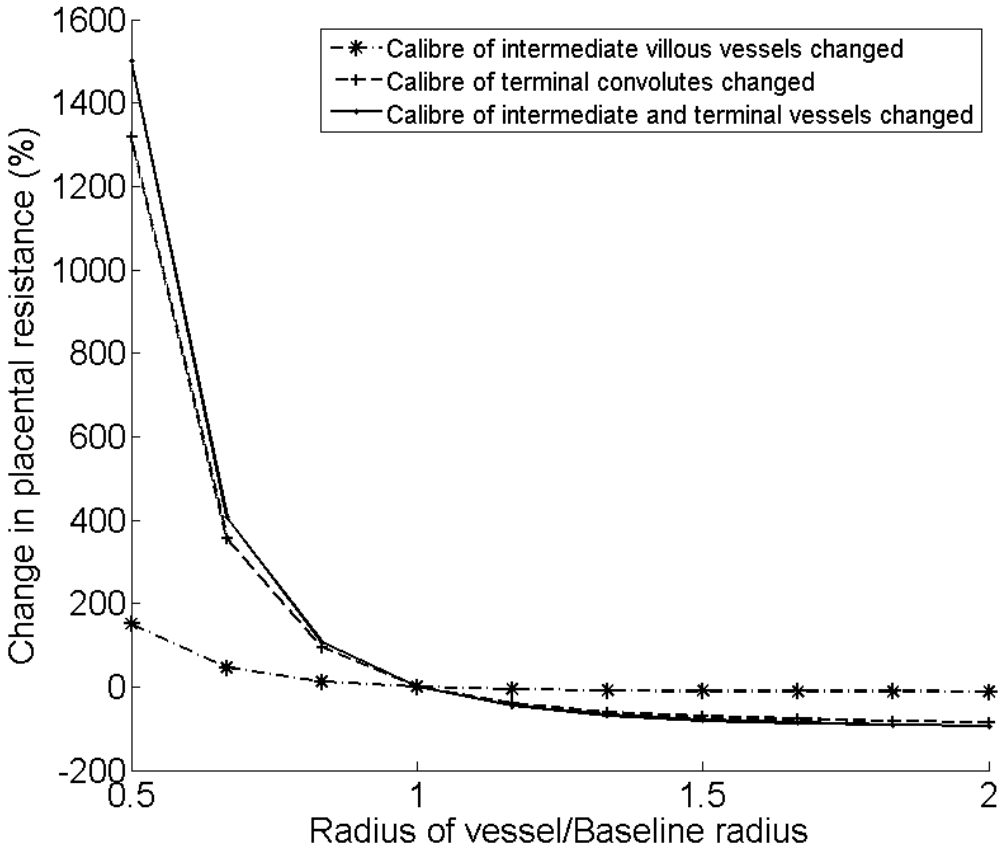

Figure 8: Model predictions on the effect of intermediate villous artery and capillary convolute calibre on feto-placental resistance. This effect is highly non-linear and a halving on capillary convolute radius has a significant impact on predicted resistance. Capillary convolute radius has the greatest effect on the resistance of the system as a whole as the placental capillaries comprise a large number of small vessels.

Short title for page headings

Multi-scale modelling of the feto-placental vasculature